New Wideband Transition From Microstrip Line to Substrate Integrated Waveguide

Zamzam Kordiboroujeni, *Student Member, IEEE*, and Jens Bornemann, *Fellow, IEEE*

***Abstract*—A new wideband transition from microstrip line to substrate integrated waveguide (SIW) is introduced. Unlike most transitions that show reduced return loss over significant parts of a regular waveguide band, the presented configuration achieves return losses better than 30 dB in standard waveguide frequency bands from X to E. The new aspect of this transition is the addition of two vias to the widely used microstrip taper transition. Moreover, the influence of the substrate height is demonstrated. The results in each frequency band are compared with the data for the regular microstrip taper alone. A design formula for the placement of the vias and taper dimensions is presented and demonstrated to provide excellent results. The structures are simulated and optimized with CST Microwave Studio. Measurements performed on a Ku-band back-to-back prototype transition demonstrate a minimum return loss of 26.05 dB and maximum insertion loss of 0.821 dB over the entire Ku-band, thus validating the design approach.**

***Index Terms*—Microstrip, substrate integrated waveguide (SIW), taper, transition, wideband.**

I. Introduction

SUBSTRATE integrated waveguide (SIW) technology has made it feasible to design low loss and low interference planar microwave structures. Transitions between SIW and other planar topologies like microstrip and coplanar waveguide (CPW) are needed in order to provide means to excite and measure these structures. More importantly, low-reflection transitions to microstrip are required to integrate and combine SIW circuits with active components such as amplifiers, e.g., [1]. In such applications, it is vital to provide low-reflection transitions so that the component design is independent of the influences of the transitions.

The first interconnect introduced is the microstrip taper [2], and it is still the most widely used type of microstrip-to-SIW transition in single-layered circuits. In [3], the design formula for this type of transition is presented and it is stated that it is generally possible to obtain a return loss (RL) better than 20 dB over the full waveguide bandwidth (∼40%) [3]. A microstrip-to-SIW transition with bandwidth of about 24% and with return loss about 15 dB for a back-to-back transition in Ku-band is presented in [4]. Another narrowband microstrip-to-SIW transition at 60 GHz in low-temperature cofired ceramic (LTCC) technology is presented in [5]. A return loss of about 15 dB in the 58–64 GHz range (about 10% bandwidth) is reported. In [6], a microstrip-to-SIW transition within a multilayered substrate is introduced. With this transition, a bandwidth of 14.5% (23.2–27.1 GHz) at 15 dB return loss is obtained. A single-layer dc-coupled microstrip-to-SIW transition using an interdigital configuration is reported in [7]. A return loss about 15 dB is achieved within a 25% bandwidth centered at 12.5 GHz. Also in 2007, another microstrip-to-SIW transition on LTCC substrate is presented [8]. The return loss for a single transition is reported as 15 dB within a 30% bandwidth. A microstrip-to-SIW transition based on an exponential instead of a linear taper is presented in [9]. The return loss is about 20 dB over a 15% bandwidth at 18 GHz. A transition between SIW and differential microstrip line in multilayered substrate is presented in [10]. Over a 10-GHz bandwidth at 35 GHz (28%) a return loss of 10 dB is achieved. In [11], different types of microstrip tapers in microstrip-to-SIW transitions are investigated and a new design approach based on electromagnetic (EM) simulation is presented. Although the resulting transitions yield return losses better than 30 dB, the structures are very narrow band (5.5% at 11 GHz). The parallel half-mode SIW (HMSIW) is suggested as transition between microstrip line and SIW structure [12]. This transition relies on the suppression of the dominant higher order TE20 mode, and hence has enhanced bandwidth compared to the conventional microstrip taper. It is stated that the proposed transition has a return loss better than 25 dB for $1.25f_c - 1.9f_c$ with $f_c = 8.6$ GHz [12]. And finally, another narrow band microstrip-to-SIW transition is presented in [13]. According to [13] and for relatively thick substrates, when the characteristic impedance of the SIW is greater than that of the microstrip, the presented transition has better performance compared to the regular microstrip taper. However, except for one case which has a return loss of about 20 dB between 15 and 40 GHz, other presented examples in [13] are narrowband.

In this paper, a new wideband microstrip-to-SIW transition is introduced. It features two vias, which have the same diameter as the SIW vias and are placed symmetrically at both sides of the microstrip taper. This transition provides return losses better than 30 dB over the entire frequency ranges of standard waveguide bands from X to E (8.2 to 90 GHz) and thus presents a significant improvement over available microstrip-to-SIW transitions.

Manuscript received March 07, 2014; revised June 08, 2014, September 22, 2014, and October 23, 2014; accepted October 26, 2014. Date of publication November 20, 2014; date of current version December 02, 2014. This work was supported by the National Science and Engineering Research Council of Canada (NSERC).

The authors are with the Department of Electrical and Computer Engineering, University of Victoria, Victoria, BC V8W 3P6, Canada (e-mail: zkordi@ece.uvic.ca; j.bornemann@ieee.org).

Color versions of one or more of the figures in this paper are available online at http://ieeexplore.ieee.org.

Digital Object Identifier 10.1109/TMTT.2014.2365794

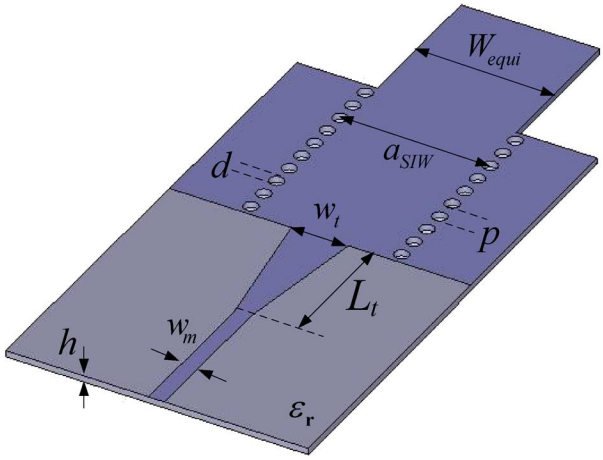

Fig. 1. Structural parameters of a single microstrip taper transition between a microstrip line and an SIW.

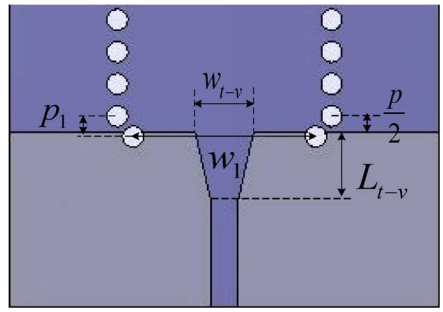

Fig. 2. Structural parameters of the new taper-via transition between microstrip line and SIW.

In Section II, details of the proposed transition and simulated data based on the optimization for a single transition in different frequency bands are presented. In each frequency band, the presented transition is compared with the regular microstrip taper, and significant improvement in return loss is achieved. In Section III, design equations for designing such transitions are proposed, and transitions designed with these formulas in two new frequency bands are presented. Results are compared with optimized data from EM software which confirm the robustness of the presented design formula. Measurement data for a Ku-band back-to-back transition are presented in Section IV and are in good agreement with simulated data. Section V concludes and provides a summary of the presented results.

II. Transition Topology

The most common type of microstrip-to-SIW transition in single-layered circuits is the microstrip taper. It not only provides acceptable return loss, but is also wideband and operates over a full waveguide bandwidth [3]. In this section, we present our new transition which improves the return loss significantly compared to the regular microstrip taper. The new transition, which consists of a microstrip taper plus two added vias, proves to be the most wideband microstrip-SIW transition available with minimum return loss.

Fig. 1 presents a single microstrip taper transition from microstrip line to SIW. The other port is terminated with a regular waveguide port.

In this figure, $a_{\rm SIW}$ is the SIW width, d is the diameter of the vias, p is the via pitch, w_m is the width of the microstrip line, $W_{\rm equi}$ is the width of the waveguide port, w_t is the taper width, L_t is the taper length, h is the substrate height, and ε_r is the relative permittivity of the substrate.

For the design of an SIW structure, the cutoff frequency f_c of the dominant mode TE_{10}, substrate permittivity ε_r and d/p ratio (which should be in the practical range of d/p ratios, i.e., $0.5 < d/p < 0.8$ [14]) are specified. The via pitch is usually chosen such that at least ten vias per guided wavelength are obtained at center frequency. The substrate thickness h is selected based on availability from manufacturers. The cutoff frequencies for the standard waveguide operating frequency bands are presented in [15]. Then the SIW width $a_{\rm SIW}$ is immediately obtained from [16] once the effective width $W_{\rm equi}$ is calculated from (1), where c is the speed of light:

$$W_{\rm equi} = \frac{c}{2f_c\sqrt{\varepsilon_r}}. \tag{1}$$

In order to excite and integrate an SIW structure with a microstrip port, the first step is to choose w_m so that the characteristic impedance of the microstrip line Z_0^{MS} becomes 50 Ω at the center frequency of the desired frequency band. Also, it should be noted that depending on the chosen h, the characteristic impedance of the SIW structure $Z_0^{\rm SIW}$ differs from 50 Ω and, therefore, different tapering topologies between microstrip line and SIW structure appear. If h is such that $Z_0^{\rm SIW} = Z_0^{MS} = 50\ \Omega$, then no taper transition is needed between the microstrip line and the SIW. This value of h can be found by deploying full-wave software optimizers. In the optimizer, we set $w_m = w_t$, and try to find h and w_m such that $|S_{11}|$ is minimum for $Z_0^{MS} = 50\ \Omega$ at the center frequency. Such h_{nt} (no-taper h) values are listed in Table I for all investigated frequency bands in this paper. However, if h is smaller or greater than h_{nt}, $Z_0^{\rm SIW}$ is smaller or greater than 50 Ω, and we will have taper-out ($w_m < w_t$) or taper-in ($w_m > w_t$) transitions, respectively. In this study, h has been chosen so that we have taper-out taper topologies ($h < h_{nt}$), as they are more common in SIW designs. Therefore, the h_{nt} values specified in Table I serve as the maximum substrate height for which the design guidelines presented in this paper apply. Note that the respective exact values of h_{nt} are not regularly available from substrate suppliers.

The new microstrip-to-SIW transition, termed taper-via transition, is presented in Fig. 2. This transition adds two vias to the conventional microstrip taper. The inserted vias are placed symmetrically at both sides of the taper and have the same dimensions as the SIW vias, so there is no need to use a different drill size in the fabrication process.

In Fig. 2, p_1 is the distance between the inserted via and the first via in the side wall of the SIW, and w_1 is the distance between the inserted vias. L_{t-v} and w_{t-v} are the length and width of the microstrip taper, respectively.

The advantage of the new configuration compared to the microstrip taper alone is that the field is more confined in lateral direction, and thus a better match from the microstrip to SIW is provided. The variations of the normalized input impedance,

TABLE I
STRUCTURAL PARAMETERS OF THE TAPER TRANSITION AND TAPER-VIA TRANSITION BETWEEN MICROSTRIP LINE AND SIW AT DIFFERENT FREQUENCY BANDS

Parameter \ Frequency band	X-band 8.2-12.4 GHz	Ku-band 12.4-18 GHz	K-band 18-26.5 GHz	Ka-band 26.5-40 GHz	U-band 40-60 GHz	E-band 60-90 GHz
f_c (GHz)	6.557	9.488	14.051	21.077	31.391	48.373
p (mm)	2.2	1.5	1	0.7	0.45	0.3
d (mm)	1.43	0.975	0.65	0.455	0.2925	0.195
a_{SIW} (mm)	14.4124	9.9502	6.7126	4.4913	3.0058	1.9545
h_{nt} (mm)	1.6623	1.2233	0.7990	0.5298	0.3616	0.2210
h (mm)	0.762	0.508	0.381	0.254	0.127	0.127
w_m (mm)	1.9161	1.2754	0.9520	0.6358	0.3213	0.3165
w_t (mm)	3.8868	2.7142	1.8881	1.2476	0.7647	0.5739
L_t (mm)	5.2611	3.7760	2.5375	1.5357	1.1104	0.6667
RL (dB)	**21.46**	**21.20**	**21.97**	**21.56**	**19.47**	**23.28**
$w_{t\text{-}v}$ (mm)	4.1697	2.7533	2.0365	1.3252	0.7784	0.6275
$L_{t\text{-}v}$ (mm)	4.2722	3.1088	1.8908	1.3168	0.9630	0.5458
w_1 (mm)	12.3678	8.4486	5.7314	3.9182	2.5078	1.7016
p_1 (mm)	1.4791	0.9494	0.6357	0.4387	0.2840	0.2417
RL (dB)	**31.53**	**35.2**	**32.6**	**31.84**	**32.19**	**29.02**

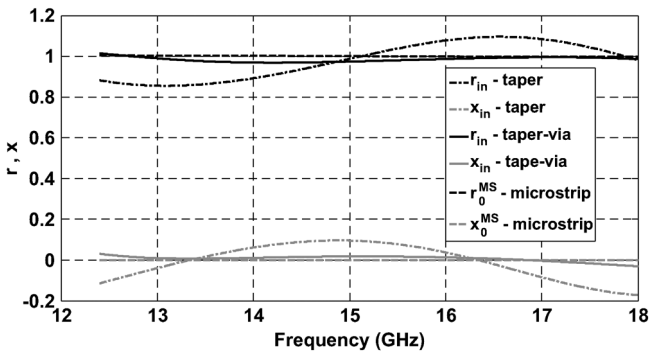

Fig. 3. Comparison between real (black) and imaginary (grey) parts of the input impedance for three different cases: structure with taper transition (dotted-dashed line), structure with taper-via transition (solid line), microstrip line (dashed line).

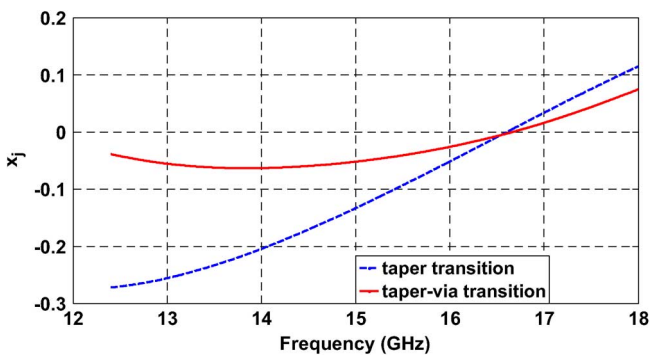

Fig. 4. Normalized reactance comparison in the microstrip-to-SIW junction plane for both taper (dashed line) and taper-via (solid line) transitions.

$z_{in} = Z_{in}/Z_0^{MS} = r_{in} + jx_{in}$, with frequency are plotted in Fig. 3 for both taper and taper-via transitions and are compared with the normalized characteristic impedance of the microstrip line. It is observed that the taper-via transition provides an input impedance closer to Z_0^{MS}, compared to the taper transition alone, which proves that better matching between the microstrip line and the SIW structure is achieved.

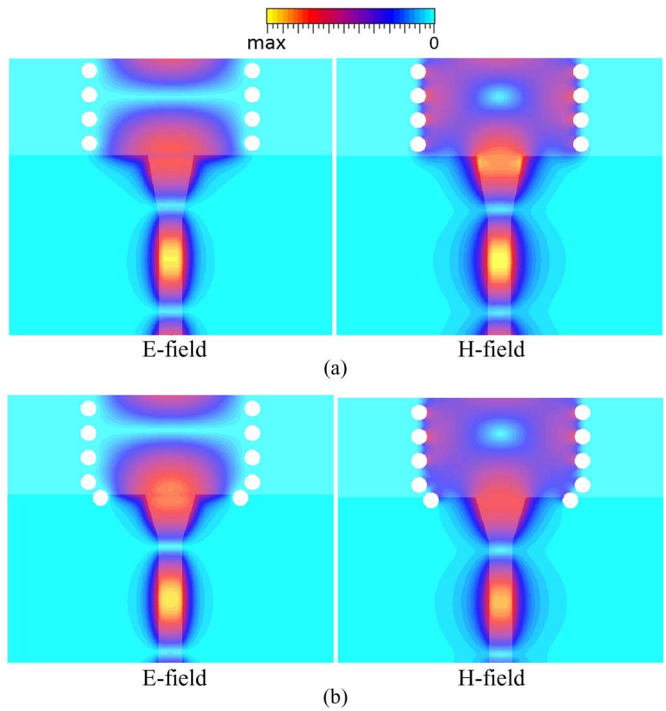

Fig. 5. Magnitudes of electric and magnetic field patterns of transitions between a microstrip line and an SIW: (a) conventional taper; (b) new transition.

In order to investigate the nature of this improved performance achieved by the proposed transition, the normalized reactance of the microstrip-to-SIW junction (x_j) is compared for both taper and taper-via transitions. As shown in Fig. 4, the added vias to the taper transition compensate the reactance effect of the microstrip taper-to-SIW transition in the junction plane and provide an overall reactance that is, over the entire bandwidth, smaller than that of the regular transition.

The field patterns in the new transition are also compared to those of the microstrip taper alone and presented in Fig. 5. In all four cases in Fig. 5, the same scaling has been adopted so that the a_{SIW} and d are exactly the same. Also, the phase of the incident wave has been chosen so that for both transitions, the

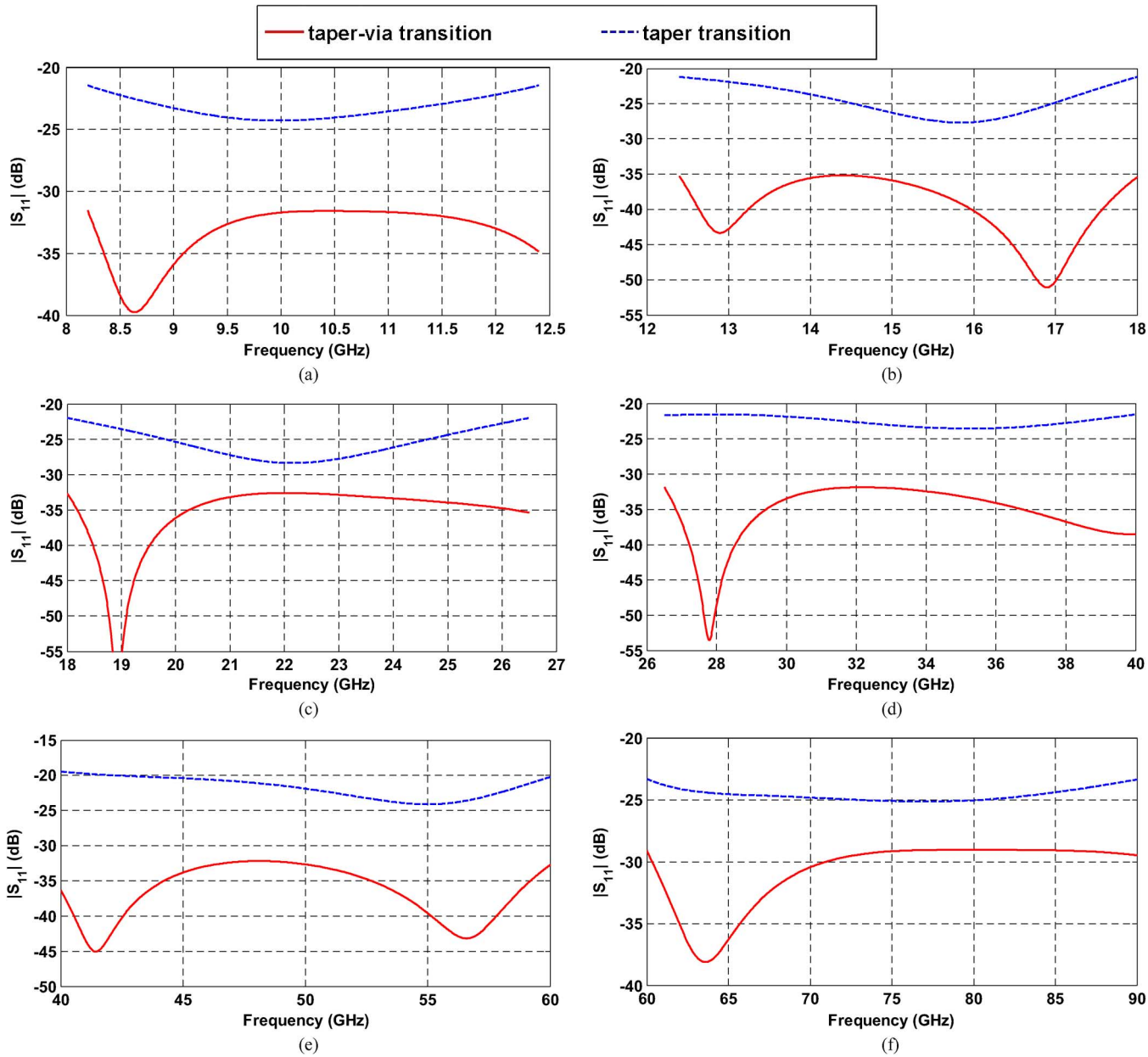

Fig. 6. Comparison between reflection coefficients of the conventional microstrip transition (taper transition—dashed line) and the new transition (taper-via transition—solid line) for different frequency bands: (a) X-band, (b) Ku-band; (c) K-band; (d) Ka-band; (e) U-band; (f) E-band; transition parameters according to Table I.

maximum E-field occurs at the beginning of the SIW structure. The H-fields are plotted at the same phase. As it is observed, by confining the field better, the new transition results in better matching between microstrip and SIW, and thus has lower return loss. When the proposed transition is deployed, the electromagnetic field of the microstrip line attaches itself better, e.g., with lower fringing fields, thus reduced lateral field extension, at the SIW interface, to the vias [Fig. 5(b)] compared to the traditional taper [Fig. 5(a)].

Based on the new configuration in Fig. 2, transitions in different microwave frequency bands from 8.2 to 90 GHz have been designed. In all cases, the performance of the new transition is compared with that of the conventional microstrip taper. The substrate material in this investigation is chosen as RT/duroid 6002 with effective permittivity $\varepsilon_r = 2.94$ for both taper and taper-via transitions. (Note that design formulas introduced in Section III can be applied to any other substrate.) The SIW structure consists of ten rows of vias. Taper-via transition parameters w_{t-v}, L_{t-v}, p_1, w_1 (cf. Fig. 2) are optimized in the frequency-domain solver of CST Microwave Studio in order to maximize the return loss of a single transition over the entire waveguide band. The optimized parameters are presented in Table I.

Optimized parameters of conventional tapers (w_t, L_t) are also presented in Table I. It is worth mentioning that the optimized parameters of the conventional tapers differ from values obtained from the formulation presented in [3]. In each frequency band, the substrate height h is chosen so that we have taper-out microstrip-SIW transitions $(h < h_{nt})$ as they are much more common than taper-in transitions. For this height

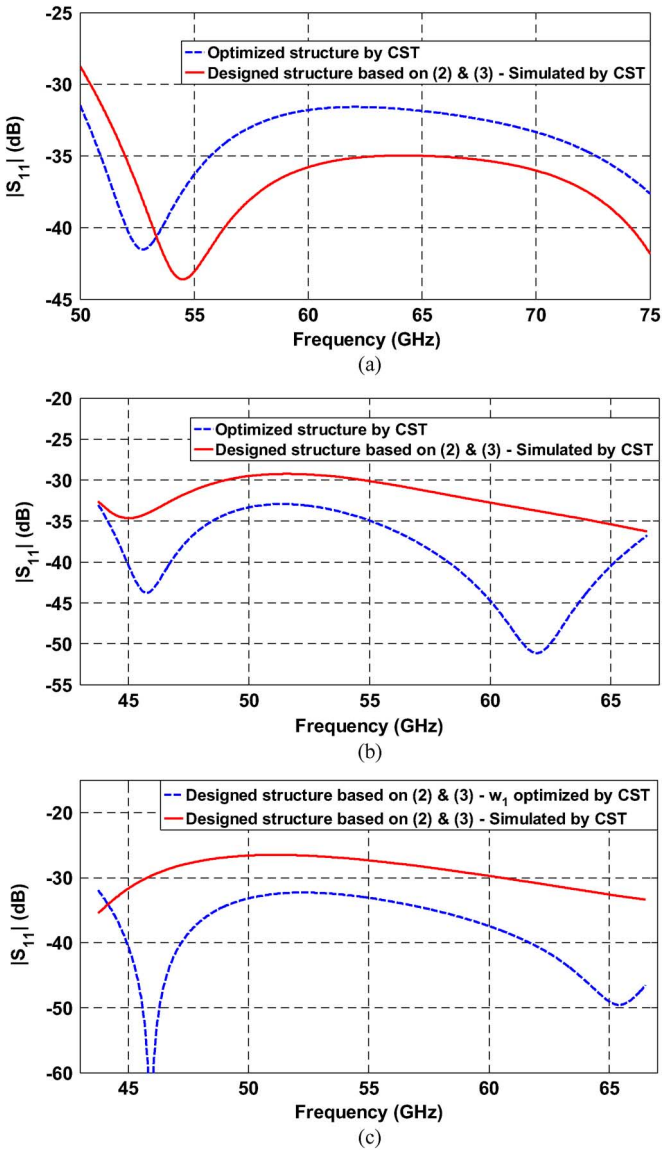

Fig. 7. Examples showing comparison between the reflection coefficient of the transition optimized in CST (blue—dashed line), and the performance of the transition designed based on (2) and (3) (red—solid line), cf. Table II: (a) Example 1; (b) Example 2; (c) Example 3.

(h), w_m is calculated so that we have $Z_0^{MS} = 50\ \Omega$ at the center frequency.

In Fig. 6, the reflection coefficients of the new transitions are compared with those of the conventional microstrip taper in each frequency band. It is observed that the new transitions show return losses better than 30 dB within each frequency band if the dielectric height is chosen properly (cf. Table I). (Note that a direct scaling process of the new transition to other bands would involve the height of the substrate material and will result in substrate heights that are not readily available from suppliers.) The new transition has significantly improved performance compared to the conventional taper transition. For the E-band, the 5 mil (0.127 mm) substrate is the only option provided by the manufacturer for maintaining $h < h_{nt}$. The new E-band transition [Fig. 6(f)] still outperforms the conventional taper transition by close to 6 dB in this case. However, if a thinner substrate is available, the performance improvement of the new transition is more significant compared to the taper alone. The minimum return loss values of all transitions in Fig. 6 are also presented in Table I.

TABLE II
STRUCTURAL PARAMETERS OF THE TAPER-VIA TRANSITION BETWEEN MICROSTRIP LINE AND SIW FOR DIFFERENT EXAMPLES

Frequency band / Parameter	Ex. 1 V-band 50-75 GHz	Ex. 2 43.75-66.5 GHz	Ex. 3 43.75-66.5 GHz
f_c (GHz)	39.875	35	35
ε_r	2.94	6.15	2.2
p (mm)	0.36	0.28	0.47
d (mm)	0.234	0.21	0.2585
a_{SIW} (mm)	2.3691	1.8947	3.0646
h (mm)	0.127	0.127	0.127
w_m (mm)	0.3184	0.1815	0.3894
$L_{t\text{-}v}^{design}$ (mm)	0.7126	0.5980	0.9141
$L_{t\text{-}v}^{CST}$ (mm)	0.7134	0.6194	0.9141
$w_{t\text{-}v}^{design}$ (mm)	0.6849	0.4747	0.8635
$w_{t\text{-}v}^{CST}$ (mm)	0.6844	0.4782	0.8635
p_1^{design} (mm)	0.2362	0.1837	0.3084
p_1^{CST} (mm)	0.2599	0.1854	0.3084
w_1^{design} (mm)	2.0269	1.6211	2.6221
w_1^{CST} (mm)	2.0173	1.6146	2.5168

III. DESIGN FORMULATION

Based on the values presented in Table I, we extract formulas for the direct design of the new transition in Fig. 2. After calculation of SIW and microstrip parameters for the desired frequency band, the next step for designing a taper-via transition is to calculate the transition parameters $w_{t-v}, L_{t-v}, p_1, w_1$ based on the following simple formulations:

$$L_{t-v} = 0.2368\lambda_{g-ms};\ w_{t-v} = w_m + 0.1547a_{\rm SIW} \quad (2)$$

$$p_1 = 0.6561p;\ w_1 = 0.8556a_{\rm SIW} \quad (3)$$

in which λ_{g-ms} is the guided wavelength of the microstrip line calculated at the center frequency

$$\lambda_{g-ms} = \frac{\lambda_{g0}}{\sqrt{\varepsilon_{reff}}}. \quad (4)$$

λ_{g0} is the wavelength in free space, and ε_{reff} is the effective dielectric constant of the microstrip line, both calculated at the center frequency. As it can be seen from (2), L_{t-v} is always close to a quarter of λ_{g-ms}. Also, the difference between w_{t-v} and w_m is approximately about one-eighth of $a_{\rm SIW}$. The placement of the two added vias is also related to SIW parameters p and $a_{\rm SIW}$ (cf. Fig. 1). Based on (2) and (3), the normalized root-mean-square errors of L_{t-v}, w_{t-v}, p_1 and w_1 to the original data in Table I are 3, 1.2, 3, and 0.6%, respectively.

Based on the proposed formulas, three examples have been investigated. Example 1 [Fig. 7(a)] presents the new taper-via transition in V-band. The d/p ratio and the substrate are chosen as in the previous structures. Examples 2 and 3 present the performances of the two new taper-via transitions at an arbitrary frequency band of between 43.75 and 66.5 GHz, where the waveguide cut-off frequency is 35 GHz. In Example 2 [Fig. 7(b)], the dielectric is chosen as RT/duroid 6006 with

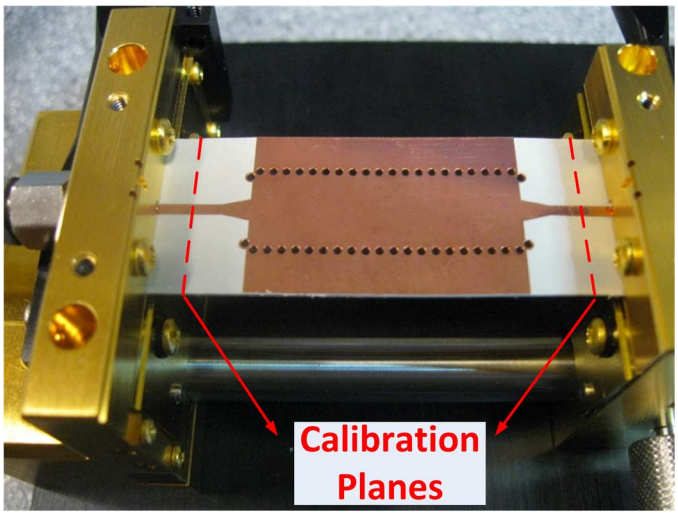

Fig. 8. Back-to-back fabricated taper-via transition at Ku-band and indication of calibration planes.

$\varepsilon_r = 6.15$ and $d/p = 0.75$, and in Example 3 [Fig. 7(c)], the dielectric is chosen as RT/duroid 5580 with $\varepsilon_r = 2.2$ and $d/p = 0.55$. In each case, the performances of the new transitions [designed from (2)–(4)] are compared with those of optimized transitions in CST.

The results are presented in Fig. 7 with structural parameters given in Table II. In this table, the structural parameters of the optimized structure by CST are presented by superscript "CST," while the values obtained from the design formulas are presented by superscript "design." It is observed that the presented design formulas result in transitions that perform close to the optimized performance [Fig. 7(a), (b)]. In some cases, however, the performance of the transition based on the design formulas is not the best possible performance (RL around 27 dB in Fig. 7(c)—solid line). A few optimization steps towards adjusting just one parameter (here w_1) will bring $|S_{11}|$ below -30 dB (dashed line in Fig 7(c)). Nevertheless, the examples presented in Fig. 7 validate the simple design formulations presented in (2), (3).

IV. Measurements

A back-to-back version of the new taper-via transition in Ku-band has been prototyped. Fig. 8 shows the fabricated structure under test. For measurements, an LRL calibration (thru-short-line) is used to deembed the influences of the test fixture and its coaxial connectors. The calibration planes are located in the feeding microstrip lines as shown in Fig. 8.

The back-to-back transition was originally designed and optimized in CST considering dielectric and conductor losses ($\tan\delta = 0.0012$, $\sigma_c = 5.8 \times 10^7$ S/m). In Fig. 9, the performance of the originally optimized structure (solid lines) is presented. The original via diameter of the Ku-band structure (cf. Table I) was changed from 0.975 mm to 0.965 mm due to drill size restrictions. Also, in the manufacturing process a minimum amount of conductor plating was necessary around the top of the left- and right-most vias. The structure is again simulated in CST including the fabrication restrictions, and its performance is presented in Fig. 9 as dashed lines for comparison with measured data (dotted lines).

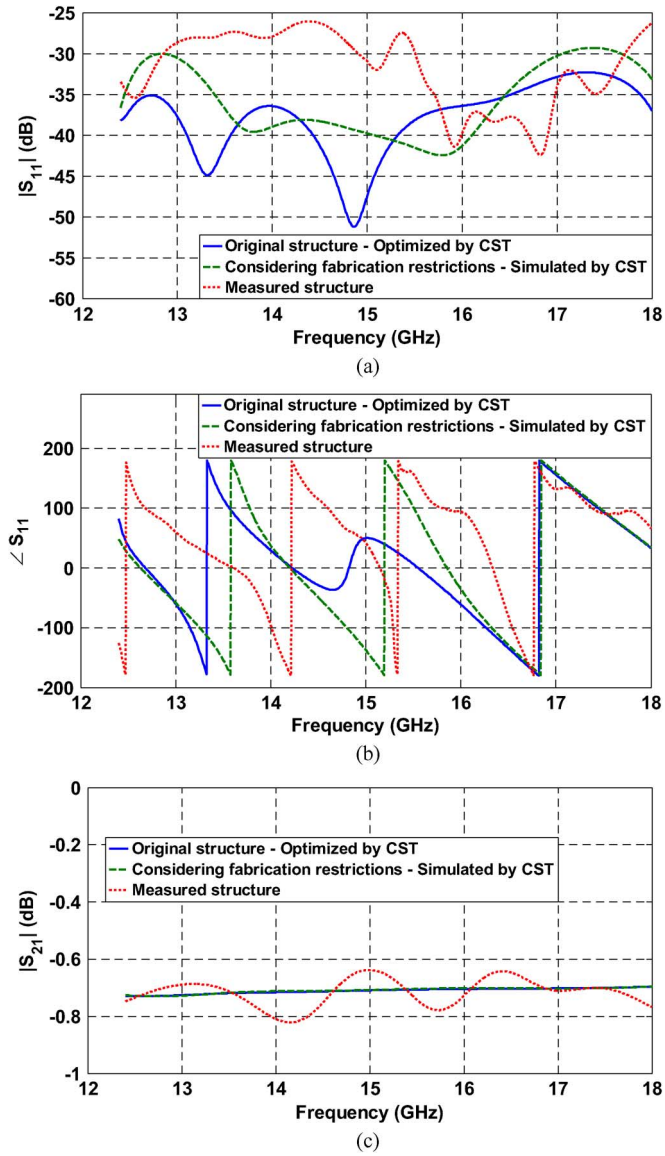

Fig. 9. Comparison between the S-parameters of the original transition optimized in CST (solid lines), the structure considering manufacturing restrictions, simulated in CST (dashed lines), and the measurement data (dotted lines): (a) reflection coefficient (amplitude); (b) reflection coefficient (phase); (c) transmission coefficient (amplitude).

It is worth mentioning that symmetric conductor plating around the outside vias is considered in the simulation, whereas the actual plated metals in the fabricated prototype are asymmetric. This is the main reason for the difference between simulated and measured results. However, the measured return loss (Fig 9(a), dotted line) is better than 26.05 dB in the entire Ku-band which, to the best of the authors' knowledge, is the lowest measured return loss over a full waveguide band for the microstrip-to-SIW transitions reported in the literature. In addition, the difference between the phases of the structures [Fig. 9(b)] is due to the different added metal plating, as it plays significant roles in the phase response [compare the data for the two simulated structures, solid line and dashed line

data, in Fig. 9(b)]. Other than that, the phases have similar patterns. The maximum measured insertion loss of the fabricated back-to-back transition is 0.821 dB [Fig. 9(c)] and is about 0.1 dB lower than the prediction by CST.

V. Conclusion

A new wideband transition from microstrip line to SIW is presented. It shows return loss values of about 30 dB over entire waveguide frequency bands, which is the lowest return loss achieved over wide frequency bands. The performance of the transition is presented in the waveguide frequency bands ranging from 8.2 to 90 GHz. The formula introduced for the design of wideband and low-reflection transitions is demonstrated to provide simplicity as well as robustness. The measured return loss for the back-to-back taper-via transition in Ku-band is better than 26.05 dB, which is the lowest measured return loss available over a full waveguide band.

We hope that this work will inspire similar improvements to other transitions between SIW and planar technologies such as CPW [17], grounded CPW [18], coplanar stripline (CPS) and slotline [19].

References

[1] M. Abdolhamidi and M. Shahabadi, "X-Band substrate integrated waveguide amplifier," *IEEE Microw. Wireless Compon. Lett.*, vol. 18, no. 12, pp. 815–817, Dec. 2008.

[2] D. Deslandes and K. Wu, "Integrated microstrip and rectangular waveguide in planar form," *IEEE Microw. Wireless Compon. Lett.*, vol. 11, no. 2, pp. 68–70, Feb. 2001.

[3] D. Deslandes, "Design equations for tapered microstrip-to-substrate integrated waveguide transitions," in *IEEE MTT-S Int. Microw. Symp. (IMS) Dig.*, Anaheim, CA, USA, May 2010, pp. 704–707.

[4] H. Nam, T.-S. Yun, K.-B. Kim, K.-C. Yoon, and J.-C. Lee, "Ku-band transition between microstrip and substrate integrated waveguide (SIW)," in *Proc. Asia-Pacific Microw. Conf. (APMC)*, Suzhou, China, Dec. 2005, pp. 1–4.

[5] T.-H. Yang, C.-F. Chen, T.-Y. Huang, C.-L. Wang, and R.-B. Wu, "A 60 GHz LTCC transition between microstrip line and substrate integrated waveguide," in *Proc. Asia-Pacific Microw. Conf. (APMC)*, Suzhou, China, Dec. 2005, pp. 1–4.

[6] Y. Ding and K. Wu, "Substrate integrated waveguide-to-microstrip transition in multilayer substrate," *IEEE Trans. Microw. Theory Tech.*, vol. 55, no. 12, pp. 2839–2844, Dec. 2007.

[7] M. Abdolhamidi, A. Enayati, M. Shahabadi, and R. Faraji-Dana, "Wideband single-layer DC-decoupled substrate integrated waveguide (SIW)—to—Microstrip transition using an interdigital configuration," in *Proc. Asia-Pacific Microw. Conf. (APMC)*, Bangkok, Thailand, Dec. 2007, pp. 1–4.

[8] C.-K. Yau, T.-Y. Huang, T.-M. Shen, H.-Y. Chien, and R.-B. Wu, "Design of 30 GHz transition between microstrip line and substrate integrated waveguide," in *Proc. Asia-Pacific Microw. Conf. (APMC)*, Bangkok, Thailand, Dec. 2007.

[9] Z. Sotoodeh, B. Biglarbegian, F. H. Kashani, and H. Ameri, "A novel bandpass waveguide filter structure on SIW technology," *Progress Electromagn. Res. Lett.*, vol. 2, pp. 141–148, 2008.

[10] F. Bauer and W. Menzel, "A wideband transition from substrate integrated waveguide to differential microstrip lines in multilayer substrates," in *Proc. 40th Eur. Microw. Conf. (EuMC)*, Paris, France, Sep. 2010, pp. 811–813.

[11] E. Miralles, H. Esteban, C. Bachiller, A. Belenguer, and V. E. Boria, "Improvement for the design equations for tapered microstrip-to-substrate integrated waveguide transitions," in *Proc. Int. Conf. Electromagn. Adv. Applicat. (ICEAA)*, Torino, Italy, Sep. 2011, pp. 652–655.

[12] D.-K. Cho and H.-Y. Lee, "A new broadband microstrip-to-SIW transition using parallel HMSIW," *J. Electromagn. Eng. Sci.*, vol. 12, no. 2, pp. 171–175, Jun. 2012.

[13] E. D. Caballero, A. B. Martinez, H. E. Gonzalez, O. M. Belda, and V. B. Esbert, "A novel transition from microstrip to a substrate integrated waveguide with higher characteristic impedance," in *IEEE MTT-S Int. Microw. Symp. (IMS) Dig.*, Seattle, WA, USA, Jun. 2013, pp. 1–4.

[14] D. Deslandes and K. Wu, "Accurate modeling, wave mechanisms, design considerations of a substrate integrated waveguide," *IEEE Trans. Microw. Theory Tech.*, vol. 54, no. 6, pp. 2516–2526, Jun. 2006.

[15] A. F. Harvey, "Standard waveguides and couplings for microwave equipment," *Proc. IEE—Part B: Radio Electron. Eng.*, vol. 102, no. 4, pp. 493–499, Jul. 1955.

[16] Z. Kordiboroujeni and J. Bornemann, "Designing the width of substrate integrated waveguide structures," *IEEE Microw. Wireless Compon. Lett.*, vol. 23, no. 10, pp. 518–520, Oct. 2013.

[17] F. Taringou, J. Bornemann, K. Wu, and T. Weiland, "Broadband interconnects between coplanar waveguide and substrate integrated waveguide for dense packaging and integration," in *IEEE MTT-S Int. Microw. Symp. (IMS) Dig.*, Tampa, FL, USA, Jun. 2014, pp. 1–3.

[18] X.-P. Chen and K. Wu, "Low-loss ultra-wideband transition between conductor-backed coplanar waveguide and substrate integrated waveguide," in *IEEE MTT-S Int. Microw. Symp. (IMS) Dig.*, Boston, MA, USA, Jun. 2009, pp. 349–352.

[19] F. Taringou, D. Dousset, J. Bornemann, and K. Wu, "Substrate-integrated waveguide transitions to planar transmission-line technologies," in *IEEE MTT-S Int. Microw. Symp. (IMS) Dig.*, Montreal, QC, Canada, Jun. 2012, pp. 1–3.

Zamzam Kordiboroujeni received the B.Sc. and M.Sc. degrees in electrical engineering from the Iran University of Science and Technology, Tehran, Iran, in 2005 and 2008, respectively. She is currently working towards the Ph.D. degree in the Department of Electrical and Computer Engineering, University of Victoria, Victoria, BC, Canada.

She is a Research Assistant in the Computer-Aided Design of Microwave Integrated Circuits (CADMIC) research group. Her current research interests include SIW technology and computational electromagnetics.

Jens Bornemann (M'87–SM'90–F'02) received the Dipl.-Ing. and the Dr.-Ing. degrees, both in electrical engineering, from the University of Bremen, Bremen, Germany, in 1980 and 1984, respectively.

From 1984 to 1985, he was a Consulting Engineer. In 1985, he joined the University of Bremen, as an Assistant Professor. Since April 1988, he has been with the Department of Electrical and Computer Engineering, University of Victoria, Victoria, BC, Canada, where he became a Professor in 1992. From 1992 to 1995, he was a Fellow of the British Columbia Advanced Systems Institute. In 1996, he was a Visiting Scientist at Spar Aerospace Limited (now MDA Space), Ste-Anne-de-Bellevue, Québec, Canada, and a Visiting Professor at the Microwave Department, University of Ulm, Germany. From 1997 to 2002, he was a codirector of the Center for Advanced Materials and Related Technology (CAMTEC), University of Victoria. In 2003, he was a Visiting Professor at the Laboratory for Electromagnetic Fields and Microwave Electronics, ETH Zurich, Switzerland. He has coauthored *Waveguide Components for Antenna Feed Systems—Theory and Design* (Artech House, 1993) and has authored/coauthored more than 300 technical papers. His research activities include RF/wireless/microwave/millimeter-wave components and systems design, and field-theory-based modeling of integrated circuits, feed networks and antennas.

Dr. Bornemann served as an Associate Editor of the IEEE Transactions on Microwave Theory and Techniques from 1999 to 2002 in the area of microwave modeling and CAD. From 2006 to 2008, he was an Associate Editor of the *International Journal of Electronics and Communications*. From 1999 to 2009, he served on the Technical Program Committee of the *IEEE MTT-S International Microwave Symposium*. He is a Registered Professional Engineer in the Province of British Columbia, Canada. He is a Fellow of the Canadian Academy of Engineering (CAE) and serves on the editorial advisory board of the *International Journal of Numerical Modelling*.